

Article

Buildup Factor Computation and Percentage Depth Dose Simulation of Tissue Mimicking Materials for an External Photon Beam (0.15–15 MeV)

Omrane Kadri ^{1,2,*}  and Abdulrahman Alfuraih ^{1,†} 

¹ Department of Radiological Sciences, College of Applied Medical Sciences, King Saud University, P.O. Box 10219, Riyadh 11433, Saudi Arabia; aalfuraih@ksu.edu.sa

² National Center for Nuclear Sciences and Technologies, Tunis 2020, Tunisia

* Correspondence: okadri@ksu.edu.sa

† These authors contributed equally to this work.

Abstract: Nowadays, the use of tissue mimicking material (TMM) is widespread in both diagnostic and therapeutic medicine, as well as for quality assurance and control. For example, patient exposure evaluation during therapeutic tests has been commonly measured using TMMs. However, only a few materials have been developed for research use at the megavoltage photon energy encountered in medical radiology. In this paper, we extended our previous work to cover the photon energy range of 0.15–15 MeV for five human tissues (adipose, cortical bone, fat, lung and muscle). As a selection criterion for TMM, other than the attenuation coefficient, we introduced the computation of the buildup factor (BUF) for a given couple of energy and depth based on the geometric progression fitting method. Hence, we developed a C⁺⁺ program able to compute BUF for depths up to 40 mean free path. Moreover, we simulated the percentage depth dose (PDD) of a 6 MV photon beam through each tissue and their equivalent materials using the Geant4 Monte Carlo toolkit (version 10.5). After the comparison of a set of parameters (mass attenuation and mass energy absorption coefficients, BUF, equivalent and effective atomic numbers, electron density, superficial and maximal dose and dose at 10 and 20 cm depths), we found that SB3 (a mixture of epoxy and calcium carbonate) and MS15 (a mixture of epoxy, phenol, polyethylene and aluminum oxide) accurately imitate cortical bone and muscle tissues, respectively. AP6 (a mixture of epoxy, phenol, polyethylene and teflon), glycerol trioleate and LN1 (a mixture of polyurethane and aluminum oxide) are also suitable TMMs for adipose, fat and lung tissues, respectively. Therefore, this work can be useful to physician researchers in dosimetry and radiological diagnosis.

Keywords: buildup factor; PDD; TMM; GP-fitting method; Geant4



Citation: Kadri, O.; Alfuraih, A. Buildup Factor Computation and Percentage Depth Dose Simulation of Tissue Mimicking Materials for an External Photon Beam (0.15–15 MeV). *Appl. Sci.* **2022**, *12*, 4250. <https://doi.org/10.3390/app12094250>

Academic Editors: Chang Ming Charlie Ma, Spyros Manolopoulos and Andrew Nisbet

Received: 4 March 2022

Accepted: 20 April 2022

Published: 22 April 2022

Publisher's Note: MDPI stays neutral with regard to jurisdictional claims in published maps and institutional affiliations.



Copyright: © 2022 by the authors. Licensee MDPI, Basel, Switzerland. This article is an open access article distributed under the terms and conditions of the Creative Commons Attribution (CC BY) license (<https://creativecommons.org/licenses/by/4.0/>).

1. Introduction

The safe usage of external photon beams in medicine requires specially designed equipment to simulate human organs, tissues and water as the reference medium. In addition to beam commissioning and dose distribution verification, this equipment also contains some dosimetry phantoms and test objects. Moreover, in order to minimize health issues related to radiation exposure, dosimetry studies have to be conducted to monitor exposure levels of individuals who handle radioactive materials and/or work in radiation exposure areas. Thus, it is important that the photon interaction cross-sections of the phantom materials match the cross-sections of the tissues. Therefore, radiation therapy tissue mimicking materials (TMMs) have been developed in recent decades [1], such as tissue and water equivalent materials, and simulation of the interaction cross-sections for modern substitutes has reached high accuracy [2]. It has been reported that various types of materials can be used as TMMs for medical applications, including nylon, polystyrene, polymethylmethacrylate (PMMA), wax, and epoxy [3–6]. Hence, in terms of radiation

response, are there any standard requirements for selecting a material as an equivalent tissue? We observed that when using international norms (IEC 2007 [7]) for ultrasound TMM development, there are no standards for MRI, surgery or thermal therapies. Furthermore, the only modality that has published guidelines on developing TMMs [8] was surgery [9]. During gamma-ray exposure, linear attenuation coefficients (LACs) are of primary importance for material selection [10], along with the effective atomic number (actual atoms of a given molecule that can be replaced by an equal number of identical (average) atoms) and the electron density (expressed in number of electrons per unit mass) [11] [12]. This manuscript can be considered as a continuation to our previous work where we introduced buildup factor (BUF) and CT numbers at 30 and 80 kVp as tuning materials to search for a photon energy interval of 0.015–0.15 MeV [13]. Nevertheless, there are no universal standards to be used for TMM selection for external irradiation by photon energies of 0.15–15 MeV.

Within the scope of this work, other tuning parameters for TMM searches will be introduced for the first time, including BUF and percentage depth dose (PDD). The buildup factor has been introduced as a correction parameter to the attenuation of a narrow monoenergetic photon beam through a thin attenuator described by the Beer–Lambert law [14] when using realistic setups. Among the many existing types and during this work, we will focus on the exposure buildup factor described by the fraction of absorbed dose in air with and without attenuator medium. In order to calculate BUFs, ANSI/ANS-6.4.3-1991 [15] tables for particle type (photon, neutron), energy, and elemental composition of the material can be used. The data were generated using five geometric progression (GP) fitting parameters based on particle energy and penetration depth as measured in mean free paths (mfp). Additionally, the central axis dose distribution inside the patient or phantom that is usually normalized to $D_{max} = 100\%$ at the depth of the dose maximum is referred to as the percentage depth dose distribution.

Our aim can be outlined as follows: (i) describing a C^{++} -based code for BUF computation, (ii) introducing the Geant4-based program (version 10.5) for PDD simulation and (iii) analyzing outputs and searching for adequate TMMs of some given human tissues. Consequently, after testing the capabilities of our simulation to reproduce the measured PDD (provided from literature) of a 6 MV photon beam within a water phantom, we carry out the calculations of BUF, PDD and some physical properties of the studied materials and tissues. As possible alternatives to adipose tissue, we are interested in AP6 (a mixture of epoxy, phenol, polyethylene and teflon), ethoxyethanol and polyethylene; aluminum, P.V.C. (polyvinylchloride), SB3 (mixture of epoxy and calcium carbonate), Teflon and Witt liquid for cortical bone tissue; Alderson fat (a mixture of polyethylene, wax and antimony trioxide), FT1 (a mixture of methylpentene and lithium carbonate) and glycerol trioleate for fat tissue; Alderson lung (a mixture of epoxy, phenol and antimony trioxide), LN1 (a mixture of polyurethane and aluminum oxide) and Stacey latex for lung tissue; and Alderson muscle 1 (a mixture of isocyanate, phenol and antimony trioxide), Alderson muscle 2, Bakelite (phenol formaldehyde), Goodman liquid (a mixture of water, glycerol and urea), Lexan (polycarbonate), M3 (a mixture of paraffin wax, magnesium oxide and calcium carbonate), Mix D (a mixture of paraffin wax, polyethylene, magnesium oxide and titanium dioxide), MS15 (a mixture of epoxy, phenol, polyethylene and aluminium oxide), MS20 (a mixture of epoxy, phenol, polyethylene and aluminum oxide), nylon 6, paraffin wax, Perspex, polystyrene, Shonka plastic (a mixture of polyethylene, nylon, carbon and calcium fluoride), Temex (a mixture of carbon, sulphur, titanium dioxide and zinc oxide) and water for muscle tissue, with all elemental compositions and material names provided by White [16]. Moreover, we will study BUF values for a photon energy interval of 0.15–15 MeV and penetration depths up to 40 mfp and PDD distributions for a realistic irradiation scenario of a 6 MV photon beam and a $5 \times 5 \text{ cm}^2$ field size. Finally, a statistical comparison will be performed to decide which TMM is most appropriate for the given tissue.

The results of this study can be considered by the radiophysics community using currently available TMM-based methods as a continual improvement to the mimicking material search procedure.

2. Materials and Methods

For the purposes of this paper, we will outline the methods used to examine the radiological properties of tissues and substitutes. Firstly, we will propose the Monte Carlo simulation procedure to calculate the PDD for a realistic external photon beam irradiation scenario. Secondly, we will describe the BUF computation method. Finally, we will enumerate other radiological parameters used for the TMM search process.

2.1. PDD Simulation

Radiation dose distribution assessment is a challenging clinical problem that requires the development of computing technologies to achieve the best clinical outcomes. As a realistic application, we carried out a simulation of the percentage depth dose distribution of a 6 MV photon beam having a field size of $10 \times 10 \text{ cm}^2$ and characterizing the output of the clinical linear accelerator Varian Clinax iX through a box phantom ($48 \times 48 \times 41 \text{ cm}^3$) located at 100 cm from the source. The box composition can be any of the studied materials. As such a procedure is time consuming, it was divided into two stages: (i) simulation of the accelerator head concluding in a phase-space file (containing particles type, energy, position, direction, . . .) and (ii) simulation of the dose distribution within the target. Thus, a schematic view of PDD computation for a linear accelerator photon beam, including the different parts of the head Linac and voxels used for dose scoring within a water phantom, is shown in Figure 1. Moreover, we used the characteristic phase-space file of the Linac provided by the Nuclear Data Section of the IAEA [17] (more than 2 GB size) and a specific interface for Geant4 simulations [18]. We scored the absorbed dose along the principal beam direction using voxels with 1 mm depth. Next, we normalized the obtained data to their maximum value. For the simulation procedure, we used the Geant4 physics list “emstandard_opt3” and the global cut-range of 1 mm for photons and electrons. Moreover, we carried out the simulation using a 40 core Dell Precision T7610 workstation equipped with an Intel Xeon E5-2680v2 CPU at 2.80 Ghz and 256 GB RAM and an 8 core Dell Precision M3800 laptop equipped with an Intel Core i7-4702HQ CPU at 2.20 Ghz and 16 GB RAM, with all of them working under the Linux operating system (Ubuntu 14.04). The statistical error related to the photon detections was less than 2% for every run carried out during this work.

2.2. BUF Computation

The computation of the buildup factor followed the three steps of (i) the calculation of the equivalent atomic number (Z_{eq}), (ii) the interpolation of the fitting parameters from existing data and (iii) the derivation of the BUF value.

Based on the total and the Compton attenuation coefficients, (μ_T/ρ) and (μ_C/ρ) (both given in cm^2/g) provided by the NIST website [19], for a photon energy from 0.15 to 15 MeV (17 standard values) and an atomic number from 1 to 92, we calculated Z_{eq} according to the following equation [20]:

$$Z_{eq} = \frac{Z_1(\log R_2 - \log R) + Z_2(\log R - \log R_1)}{\log R_2 - \log R_1} \quad (1)$$

where R represents the fraction (μ_C/μ_T) of the compound in consideration and R_1 and R_2 are the fractions of the two nearest elements with atomic numbers Z_1 and Z_2 . Since the atomic number for composite materials is not represented by a single number across an entire energy range similarly to pure elements, they can be represented by Z_{eq} .

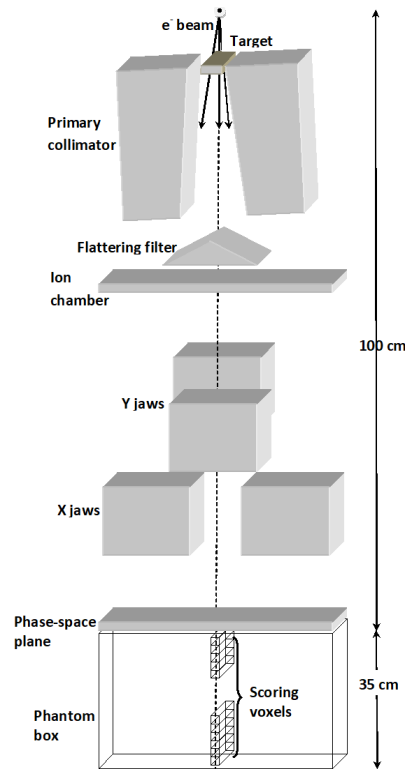


Figure 1. Typical schematic view of PDD calculation for a linear accelerator photon beam in a water phantom. The different parts of the head Linac and the voxels used to score the dose within the box are shown.

On the other hand, the five GP-fitting parameters (a, b, c, d and X_k) are dependent on Z_{eq} and photon energy. Hence, we calculated each parameter using the data provided by the ANSI/ANS-6.4.3-1991 report for 23 elements and 25 photon energies using the following logarithmic interpolation formula:

$$F = \frac{F_1(\log Z_2 - \log Z_{eq}) + F_2(\log Z_{eq} - \log Z_1)}{\log Z_2 - \log Z_1} \tag{2}$$

where F_1 and F_2 represents the values of GP-fitting parameters corresponding to Z_1 and Z_2 , respectively. F can be any of the five parameters. Eventually, the GP form of the BUF as a function of depth, expressed in mean free paths X (defined as the inverse of the linear attenuation coefficient), can be expressed as follows:

$$\frac{B(X) - 1}{b - 1} = \begin{cases} \frac{K^X - 1}{K - 1} & \text{if } K \neq 1 \\ X & \text{if } K = 1 \end{cases} \tag{3}$$

where K represents the geometric progression term. Here, we can see the reason for the GP formula nomination, as the second term of Equation (3) represented the sum of K^n for n varying from 0 to X . For $X \leq 40$ mfp, K can be written in the following way:

$$K(X) = cX^a + d \frac{\tanh(X/X_k - 2) - \tanh(-2)}{1 - \tanh(-2)} \tag{4}$$

For a fixed material and photon energy, the BUF computation procedure was based on the calculation of Z_{eq} , using the Equation (1), followed by the interpolation of the GP-fitting parameters (a, b, c, d and X_k) calculated using Equation (2) and plugged into Equations (3) and (4).

During this work, we computed BUF for 5 tissues and 30 TMM candidates. Table 1 illustrated the elemental composition of the studied materials and tissues. For each stud-

ied case, the photon energy range of 0.15–15 MeV and the penetration depth range of 0.5–40 mfp were represented by 17 standard energies and 17 standard depths, resulting in 289 values of BUF. More explanations were given within our previous work [13].

Table 1. Percentage elemental composition and equivalent atomic number (for three photon energies in MeV) of studied tissues and their mimicking material candidates.

Material	Elemental Composition	Z_{eq}		
		0.5	5	15
Adipose	H(12.001), C(64.005), N(0.800), O(22.902), Na(0.050), Mg(0.002) P(0.016), S(0.070), Cl(0.120), K(0.030), Ca(0.002), Fe(0.002)	6.67	5.374	5.348
AD1	H(8.359), C(69.133), N(2.360), O(16.938), F(3.070), Cl(0.140)	6.713	5.656	5.619
AD2	H(11.180), C(53.310), O(35.510)	6.914	5.635	5.597
AD3	H(14.370), C(85.630)	5.928	4.742	4.705
Bone	H(3.392), C(15.509), N(3.972), O(44.128), Na(0.060), Mg(0.210) P(10.206), S(0.310), Ca(22.213)	14.08	10.49	10.44
CB1	Al(100.000)	13	13	13
CB2	H(4.840), C(38.436), Cl(56.724)	14.51	11.38	11.32
CB3	H(3.100), C(31.260), N(0.990), O(37.570), Cl(0.050), Ca(27.030)	14.27	10.11	10.06
CB4	C(24.020), F(75.980)	8.653	8.251	8.243
CB5	H(4.686), O(56.630), P(10.867), K(27.817)	14.11	10.94	10.88
Fat	H(12.210), C(76.080), O(11.710)	6.007	5.127	5.111
FA1	H(14.369), C(85.607), O(0.004), Sb(0.020)	6.382	4.749	4.71
FA2	H(11.701), Li(3.48), C(72.748), O(12.071)	6.775	5.09	5.076
FA3	H(11.840), C(77.320), O(10.840)	6.774	5.141	5.126
Lung	H(10.134), C(10.237), N(2.866), O(75.752), Na(0.184), Mg(0.007) Al(0.001), P(0.082), S(0.225), Cl(0.266), K(0.194), Ca(0.010) Fe(0.041), Zn(0.001)	8.153	6.576	6.547
LU1	H(5.741), C(73.947), N(2.010), O(18.142), Sb(0.160)	9.129	5.873	5.821
LU2	H(6.000), C(51.440), N(4.290), O(30.720), Al(7.550)	8.231	6.536	6.511
LU3	H(10.100), B(8), C(79.200), O(0.120), S(1.910), Zn(0.670)	8.843	5.325	5.298
Muscle	H(10.200), C(12.300), N(3.500), O(72.893), Na(0.080) Mg(0.020), P(0.200), S(0.500), K(0.300), Ca(0.007)	8.075	6.534	6.506
MU1	H(8.830), C(64.450), N(4.050), O(20.350), Cl(2.240), Sb(0.080)	8.908	5.843	5.79
MU2	H(8.871), C(66.817), N(3.100), O(21.132), Sb(0.080)	8.037	5.63	5.593
MU3	H(5.740), C(77.460), O(16.800)	6.438	5.771	5.73
MU4	H(10.200), C(12.010), N(3.540), O(74.250)	7.505	6.459	6.435
MU5	H(5.549), C(75.573), O(18.878)	6.526	5.827	5.783
MU6	H(11.430), C(65.580), O(9.220), Mg(13.480), Ca(0.290)	8.287	5.891	5.833
MU7	H(13.401), C(77.799), O(3.500), Mg(3.860), Ti(1.440)	8.436	5.274	5.247
MU8	H(9.750), C(63.160), N(0.940), O(16.020), Al(9.600), Cl(0.530)	8.437	6.06	6.045
MU9	H(8.119), C(58.344), N(1.780), O(18.638), Mg(13.029), Cl(0.090)	8.316	6.338	6.317
MU10	H(9.799), C(63.683), N(12.379), O(14.139)	6.364	5.48	5.452
MU11	H(14.860), C(85.140)	5.902	4.706	4.67
MU12	H(8.051), C(59.986), O(31.963)	6.918	5.843	5.796
MU13	H(7.74), C(92.26)	6.301	5.284	5.267
MU14	H(10.2), C(76.8), N(3.6), O(5.9), F(1.7), Ca(1.8)	8.043	5.489	5.456
MU15	H(9.654), C(87.489), N(0.06), O(0.473), S(1.539) Ti(0.332), Zn(0.453)	8.42	5.407	5.377
MU16	H(11.19), O(88.81)	7.72	6.505	6.478

2.3. Analysis Procedure

Other physical parameters were evaluated for tissues and TMMs. Among them, we used the NIST database to calculate the mass attenuation coefficient (μ/ρ) and the mass energy absorption coefficient (μ_{en}/ρ) according to the additivity rule [21] as follows:

$$\frac{\mu}{\rho} = \sum_i w_i \left(\frac{\mu}{\rho}\right)_i \tag{5}$$

where w_i represents the fraction by weight of the i th element of the material.

Additionally, we investigated two other parameters useful for dose calculation (diagnosis/therapy) called the effective atomic number (Z_{eff}), defined as the weighted average of the number of electrons per atom in a composite material and the effective electron number N_{eff} , which is defined by the number of electrons per unit of mass.

Such parameters are given by [13]:

$$Z_{eff} = \frac{\sum_i f_i A_i (\frac{\mu}{\rho})_i}{\sum_i f_i \frac{A_i}{Z_i} (\frac{\mu}{\rho})_i} \quad (6)$$

and

$$N_{eff} = N_A \frac{Z_{eff}}{\sum_i n_i A_i} \quad (7)$$

where A_i , Z_i , f_i and n_i are the atomic mass, the atomic number, the molar fraction and the number of atoms of the i th element and N_A the Avogadro number (602.214×10^{21}), respectively.

After calculating all needed parameters, we derived the percentage of the relative difference between each tissue and TMM candidate values. The computation of the different parameters was performed with an in-house C++ based program executed under the Ubuntu operating system.

3. Results and Discussion

Figure 2 shows the comparison of the Geant4-simulated and experimental PDD data for a 6 MV photon beam, $3 \times 3 \text{ cm}^2$ field size and an 100 cm source-to-surface distance (SSD) through water medium. With a statistical error related to the simulation of about 2% and an experimental error of about 2%, we can observe the good agreement of both distributions. Moreover, we confirm the ability of Geant4 to reproduce a PDD distribution for similar situations, as already carried out in the literature [22–24]. Such good agreement allowed us to safely proceed with the present method of the PDD simulation for other materials than water medium. Table 2 lists the radiological properties of the studied tissues, including Z_{eq} , μ/ρ , μ_{en}/ρ , Z_{eff} and the GP-fitting parameters of the BUF for a photon energy between 0.15 and 15 MeV.

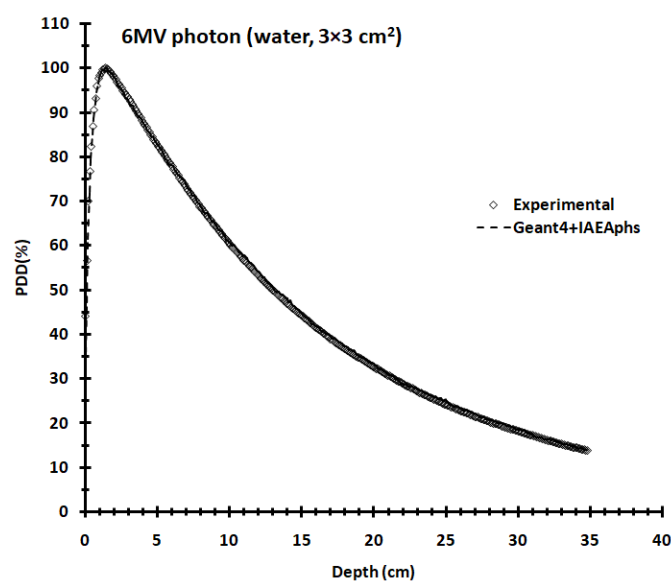


Figure 2. Comparison of Geant4-simulated (based on IAEA phase space file) and experimental PDD data for a 6 MV photon beam (field size of $3 \times 3 \text{ cm}^2$) within water.

Table 2. Physical properties of the studied tissues: GP-fitting parameters of the BUF (a, b, c, d and X_k), equivalent atomic number (Z_{eq}), mass attenuation coefficient (μ/ρ), mass energy absorption coefficient (μ_{en}/ρ) in cm^2/g and effective electron density ($\times 10^{-23}$) at different photon energies between 0.15 and 15 MeV.

		0.15	0.2	0.3	0.4	0.5	1	1.5	2	3	5	10	15
Adipose	a	-0.222	-0.217	-0.190	-0.172	-0.154	-0.100	-0.077	-0.048	-0.016	0.018	0.041	0.047
	b	4.117	3.517	3.022	2.746	2.575	381.555	2.046	1.931	1.772	1.590	1.379	1.282
	c	2.600	2.507	2.230	2.047	1.890	1.496	1.345	1.204	1.065	0.935	0.854	0.834
	d	0.099	0.095	0.082	0.073	0.067	0.046	0.041	0.025	0.009	-0.010	-0.019	-0.026
	X_k	14.121	13.923	14.174	13.864	14.149	13.909	13.740	14.253	12.433	14.772	13.016	14.469
	Z_{eq}	6.626	6.640	6.658	6.662	6.670	6.664	5.428	5.394	5.383	5.374	5.362	5.348
	μ/ρ	0.151	0.137	0.119	0.107	0.097	0.071	0.058	0.050	0.040	0.030	0.021	0.018
	μ_{en}/ρ	0.027	0.030	0.032	0.033	0.033	0.031	0.029	0.026	0.023	0.019	0.015	0.014
	Z_{eff}	2.999	2.991	2.987	2.985	2.984	2.983	2.985	2.991	3.014	3.073	3.242	3.397
	N_{eff}	1.546	1.542	1.540	1.539	1.539	1.538	1.539	1.542	1.554	1.585	1.671	1.751
Bone	a	-0.041	-0.056	-0.078	-0.081	-0.080	-0.063	-0.049	-0.034	-0.011	0.016	0.042	0.062
	b	2.722	2.661	2.482	2.353	2.250	1.978	1.874	1.798	1.687	1.539	1.349	1.263
	c	1.266	1.365	1.468	1.471	1.453	1.323	1.234	1.155	1.056	0.955	0.875	0.826
	d	-0.007	-0.006	0.014	0.016	0.018	0.019	0.017	0.012	0.001	-0.019	-0.032	-0.053
	X_k	10.507	7.952	16.942	15.907	16.301	15.937	14.926	14.499	10.770	15.083	13.319	14.462
	Z_{eq}	14.088	14.172	14.022	14.063	14.082	14.102	11.402	10.753	10.572	10.486	10.449	10.437
	μ/ρ	0.148	0.131	0.111	0.099	0.090	0.066	0.053	0.046	0.037	0.029	0.023	0.021
	μ_{en}/ρ	0.032	0.030	0.030	0.031	0.031	0.029	0.026	0.024	0.021	0.019	0.016	0.016
	Z_{eff}	6.258	6.122	6.041	6.015	6.004	5.990	5.994	6.019	6.102	6.315	6.860	7.300
	N_{eff}	1.733	1.696	1.673	1.666	1.663	1.659	1.660	1.667	1.690	1.749	1.900	2.022
Fat	a	-0.217	-0.213	-0.211	-0.192	-0.171	-0.110	-0.081	-0.049	-0.017	0.018	0.041	0.048
	b	4.062	3.471	3.147	2.842	2.656	1191.250	2.064	1.946	1.780	1.596	1.382	1.285
	c	2.545	2.470	2.412	2.196	2.010	1.544	1.361	1.210	1.067	0.934	0.853	0.831
	d	0.097	0.093	0.094	0.080	0.079	0.053	0.045	0.027	0.010	-0.010	-0.018	-0.025
	X_k	14.117	13.694	14.409	13.472	14.190	13.780	13.764	14.372	12.632	14.888	13.289	14.154
	Z_{eq}	6.763	6.774	6.002	6.004	6.007	6.001	5.162	5.140	5.132	5.127	5.121	5.111
	μ/ρ	0.151	0.138	0.119	0.107	0.098	0.071	0.058	0.050	0.040	0.030	0.021	0.018
	μ_{en}/ρ	0.027	0.030	0.032	0.033	0.033	0.031	0.029	0.026	0.023	0.019	0.015	0.013
	Z_{eff}	2.931	2.925	2.922	2.920	2.920	2.919	2.920	2.926	2.947	3.000	3.153	3.294
	N_{eff}	1.585	1.582	1.580	1.580	1.579	1.579	1.579	1.583	1.594	1.623	1.705	1.782
Lung	a	-0.161	-0.167	-0.152	-0.139	-0.126	-0.083	-0.061	-0.041	-0.014	0.018	0.039	0.047
	b	3.856	3.307	2.859	2.621	2.468	2.093	1.981	1.873	1.731	1.567	1.366	1.273
	c	2.054	2.073	1.932	1.815	1.713	1.414	1.282	1.182	1.060	0.940	0.865	0.841
	d	0.063	0.066	0.058	0.053	0.048	0.033	0.027	0.019	0.005	-0.012	-0.022	-0.032
	X_k	14.487	14.052	14.196	14.240	14.239	14.432	14.473	13.965	13.183	13.953	13.409	15.140
	Z_{eq}	8.079	8.093	8.128	8.144	8.153	8.156	6.682	6.608	6.592	6.576	6.550	6.547
	μ/ρ	0.149	0.136	0.118	0.105	0.096	0.070	0.057	0.049	0.039	0.030	0.022	0.019
	μ_{en}/ρ	0.027	0.029	0.032	0.032	0.033	0.031	0.028	0.026	0.023	0.019	0.016	0.014
	Z_{eff}	3.493	3.479	3.470	3.466	3.465	3.464	3.465	3.476	3.510	3.599	3.847	4.071
	N_{eff}	1.482	1.476	1.473	1.471	1.470	1.470	1.470	1.475	1.489	1.527	1.632	1.727
Muscle	a	-0.163	-0.168	-0.153	-0.140	-0.127	-0.084	-0.062	-0.042	-0.014	0.018	0.039	0.047
	b	3.874	3.317	2.866	2.625	2.471	2.096	1.983	1.875	1.733	1.568	1.367	1.273
	c	2.067	2.086	1.941	1.822	1.718	1.416	1.284	1.183	1.060	0.940	0.865	0.841
	d	0.064	0.067	0.059	0.054	0.048	0.033	0.028	0.019	0.005	-0.012	-0.021	-0.032
	X_k	14.481	14.035	14.198	14.214	14.219	14.390	14.423	13.967	13.099	13.991	13.333	15.149
	Z_{eq}	8.010	8.022	8.053	8.067	8.075	8.076	6.637	6.564	6.549	6.534	6.509	6.506
	μ/ρ	0.149	0.136	0.118	0.105	0.096	0.070	0.057	0.049	0.039	0.030	0.022	0.019
	μ_{en}/ρ	0.027	0.029	0.032	0.032	0.033	0.031	0.028	0.026	0.023	0.019	0.016	0.014
	Z_{eff}	3.471	3.458	3.450	3.446	3.444	3.443	3.444	3.455	3.488	3.576	3.822	4.043
	N_{eff}	1.483	1.477	1.473	1.472	1.471	1.471	1.471	1.476	1.490	1.527	1.632	1.727

3.1. Adipose Tissue

- PDD distribution: Figure 3 shows the Geant4-simulated percentage depth dose distributions for the five studied tissues for a $10 \times 10 \text{ cm}^2$ field size for a 6 MV photon beam. The PDD distribution is a function of depth, field size and SSD and can be characterized by the surface dose ($d_0(\%)$), depth of maximum dose ($d_{\text{max}}(\text{cm})$) 80% dose ($d_{80\%}(\text{cm})$), and dose at depth of 10 cm ($d_{10\text{cm}}(\%)$) and 20 cm ($d_{20\text{cm}}(\%)$). We can see a fast increase followed by a slower decrease after reaching the maximum photon absorption. The first region is caused by the backscattering dominance, whereas the second region simply describes the exponential attenuation of photons through matter;
- Photon energy effect: The incident photon energy dependence of adipose tissue BUF for fixed penetrations of 0.5, 5, 15, 25 and 40 mfp is shown in Figure 4 (left side). For each penetration depth, BUF continuously decreased as a function of energy. In order to understand such phenomena, the studied energy interval can be divided into two subintervals: from 0.15 to 1 MeV corresponding to the Compton process domination and from 1 to 15 MeV, where the pair production effect is dominant. The large value of the BUF at the beginning of each curve can be explained by the multiple Coulomb scattering, which only attenuates and does not totally absorb the photon energy, existing for a longer time in the medium. Similarly to the photoelectric effect, resulting in lower BUF values due to the total energy absorption, the second energy interval is mainly dominated by the pair production process;
- Penetration depth effect: Figure 4 (right side) shows the dependence of BUF on penetration depth dependence for fixed photon energies of 0.2, 0.5, 1, 1.5, 5, 10 and 15 MeV for adipose tissue. Generally, increased BUF values for deeper penetrations were observed. However, the increasing rate of BUF (comparing 0.5 to 40 mfp range edges) is inversely proportional to photon energies. Additionally, we can see the contribution effect of secondary photons to BUF due to the multiple scattering effect, which reaches a maximum at 1 MeV;
- Chemical composition effect: A major effect on the BUF magnitude is caused by the difference in the chemical compositions of adipose tissue and the equivalent candidate materials. Figure 5 shows the relative BUF deviations of AD1, AD2 and AD3 to adipose tissue as a function of energy at fixed penetrations of 0.5, 15 and 40 mfp and as a function of mfp at selected photon energies (0.5, 5 and 15 MeV). According to the photon energy region, the magnitude of the build-up factor and its dependence on Z_{eq} vary. As the relative deviation of BUFs are given in terms of $\delta(\%) = 100 \times (1 - \text{BUF}(\text{Material})/\text{BUF}(\text{Adipose}))$ in Figure 5, we have: $\text{BUF}(\text{AD2}) > \text{BUF}(\text{AD1}) > \text{BUF}(\text{Adipose}) > \text{BUF}(\text{AD3})$, and from Table 1, we have $Z_{\text{eq}}(\text{AD2}) < Z_{\text{eq}}(\text{AD1}) < Z_{\text{eq}}(\text{Adipose}) < Z_{\text{eq}}(\text{AD3})$, which confirms the theoretical hypothesis that BUF and Z_{eq} are inversely proportional;
- TEM study: Based on the relative difference between the radiological properties of tissues and mimicking material candidates in % for BUF, Z_{eq} , μ/ρ , μ_{en}/ρ , Z_{eff} , N_{eff} , d_0 and d_{max} and in cm for d_{80} , $d_{10\text{cm}}$ and $d_{20\text{cm}}$ listed in Table 3 and plotted in Figure 5, we can see the close similarity of the AD1 candidate to adipose tissue. Moreover, the substitute AD2 seems to be closer to adipose tissue when looking for other parameters than BUF and Z_{eq} . However, the discrepancy of AD3 compared to adipose tissue was seen for many parameters. Therefore, AD1 can be an acceptable TMM for adipose for the actual photon energy range.

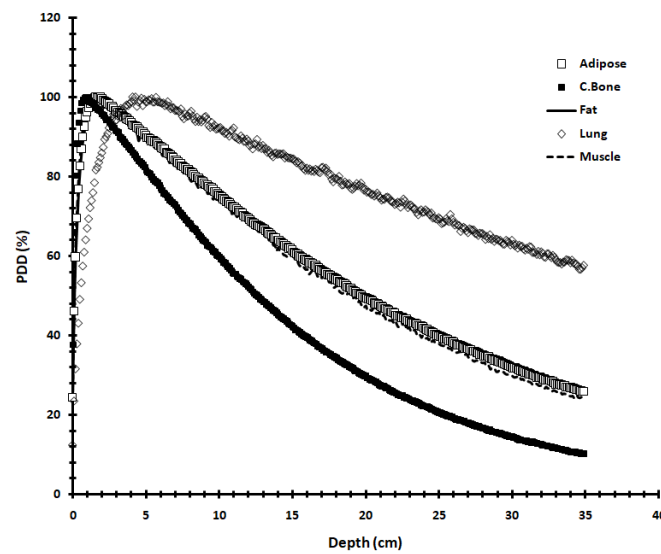


Figure 3. Geant4-simulated PDD of adipose, cortical bone, fat, lung and muscle tissues for a $10 \times 10 \text{ cm}^2$ field size of a 6 MV photon beam.

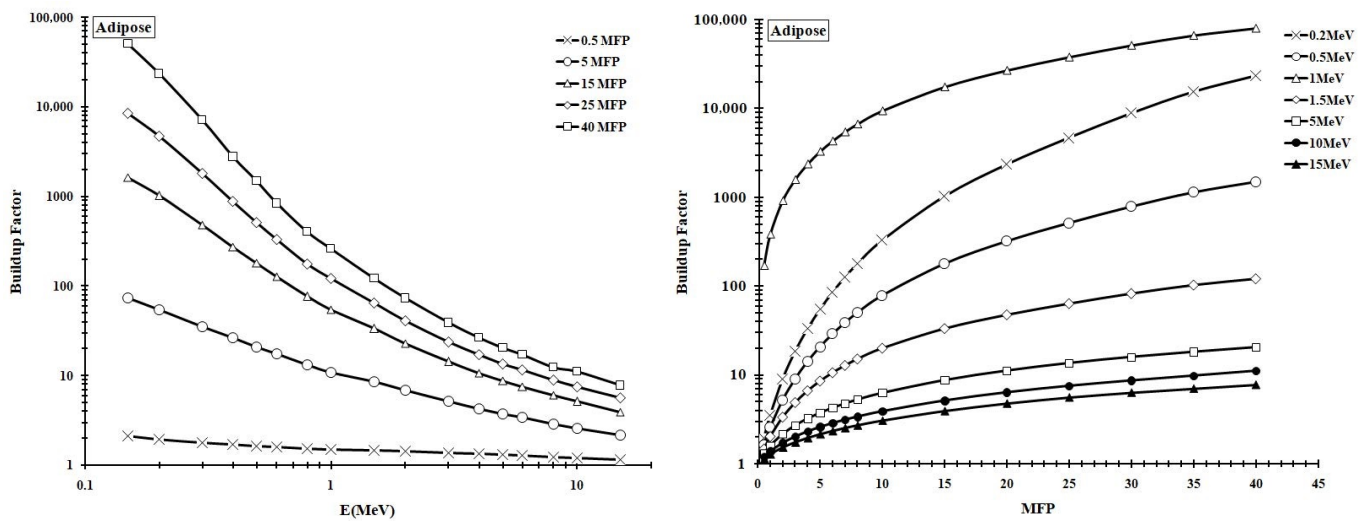


Figure 4. Buildup factor for adipose tissue as a function of: (left side) photon energy for fixed depths between 0.5 and 40 mfp and (right side) depth for a fixed photon energy between 0.15 and 15 MeV.

3.2. Cortical Bone Tissue

Generally, the effects of the penetration depth, the photon energy and the chemical composition on BUFs for cortical bone are similar to the adipose case study. Moreover, we can see from Figure 6, which shows the energy and the penetration depth effects on BUF for cortical bone tissue, that the previously described dependence as a function of Z_{eq} remains valid. Additionally, from Figure 7 and Table 3, which present the relative percentage deviation of BUF and PDD for candidate materials for cortical bone, we can observe the usual similarities between CB3 and cortical bone. Accordingly, CB3 can be used in medical imaging, dosimetry and radiotherapy as a TMM that precisely models cortical bone tissue.

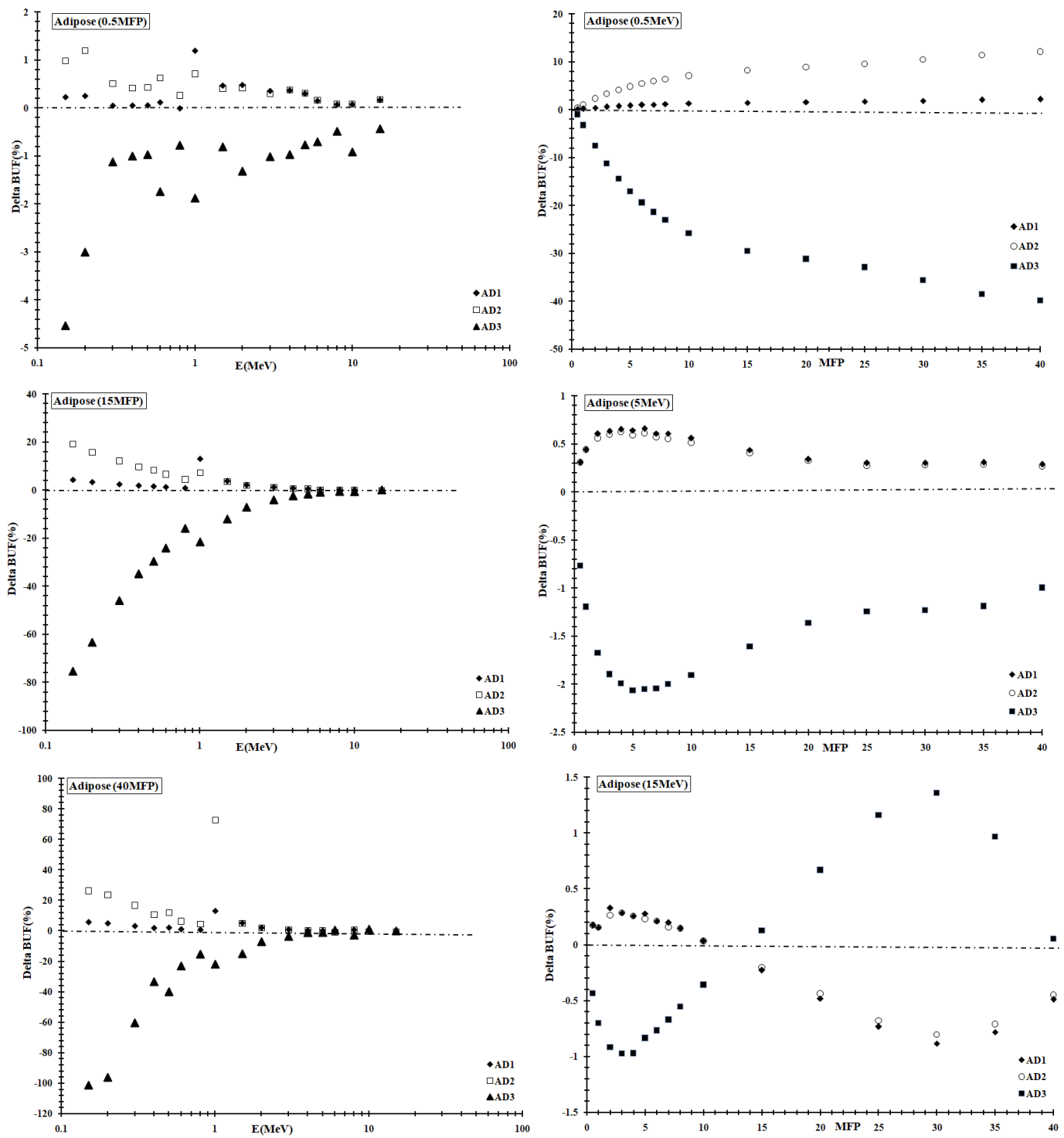


Figure 5. Relative percentage deviation of BUF values of substitute materials for adipose tissue as a function of: (left side) photon energy for fixed depths of 0.5, 15 and 40 mfp and (right side) depth for fixed photon energies of 0.5, 5 and 15 MeV.

Table 3. Relative difference between tissues and mimicking material candidate properties in % for BUF, Z_{eq} , μ/ρ , μ_{en}/ρ , Z_{eff} , N_{eff} , d0 and dmax and in cm for d80, d10cm and d20cm. Here, d0, dmax, d80, d10cm and d20cm are represented as the superficial, maximum, 80% of the maximum, and depth of 10 cm and 20 cm adsorbed dose, respectively.

Tissue	Material	BUF	Z_{eq}	μ/ρ	μ_{en}/ρ	Z_{eff}	N_{eff}	d0(%)	dmax(cm)	d80%(cm)	d10cm(%)	d20cm(%)
Adipose	AD1	1.9	3.1	3.1	3.1	17.0	13.3	1.6	0.3	0.3	0.3	2.0
	AD2	8.0	4.3	0.6	0.6	4.9	0.5	0.8	0.0	-0.1	0.1	0.0
	AD3	26.0	11.5	1.6	1.6	10.8	0.3	0.8	0.0	-0.1	1.1	2.0
Bone	CB1	6.9	15.6	5.0	5.5	108.5	68.0	23.6	-0.3	-1.1	19.1	33.9
	CB2	4.2	5.7	0.7	0.9	9.6	20.7	14.3	0.2	1.2	15.6	33.2
	CB3	0.6	2.3	0.3	0.4	2.1	2.4	1.1	0.1	-0.2	0.0	0.3
	CB4	78.8	29.9	8.9	9.9	28.6	61.4	0.5	0.1	-0.3	2.5	6.7
	CB5	0.6	2.4	0.9	0.9	5.8	12.3	2.4	0.3	0.1	3.0	5.7
Fat	FA1	10.8	7.1	1.5	1.6	8.7	2.7	0.0	0.3	0.0	2.3	0.6
	FA2	9.9	4.9	0.9	0.9	0.4	1.4	2.9	0.0	0.0	1.9	1.0
	FA3	9.8	4.7	0.3	0.3	1.3	1.3	0.4	0.2	0.0	0.5	0.2
Lung	LU1	5.7	11.2	4.6	4.5	14.8	32.3	6.5	0.4	-1.3	2.6	5.7
	LU2	0.5	0.8	4.0	4.0	18.8	22.3	7.3	0.5	-0.2	0.2	0.4
	LU3	4.8	13.5	1.8	1.8	10.2	10.3	7.3	1.2	-0.1	0.4	0.0
Muscle	MU1	4.3	9.8	1.9	1.9	0.6	11.8	2.3	0.0	0.0	3.1	0.2
	MU2	2.1	8.0	2.0	2.1	1.5	15.4	4.2	-0.2	0.0	2.1	0.8
	MU3	28.4	15.7	4.7	4.8	14.8	34.4	8.4	0.0	-0.7	7.2	12.0
	MU4	6.1	3.9	0.1	0.1	0.2	1.0	2.3	-0.4	-0.4	4.4	4.6
	MU5	25.7	14.8	4.8	5.0	16.5	35.2	6.9	0.1	-0.7	5.6	9.3
	MU6	1.8	6.4	0.8	0.9	10.3	1.6	1.9	0.0	0.0	2.0	2.1
	MU7	3.3	12.0	2.2	2.3	19.1	2.2	1.9	-0.3	-0.1	1.9	1.7
	MU8	2.4	5.8	1.2	1.2	3.4	3.5	2.7	0.2	0.1	3.2	1.3
	MU9	1.5	2.9	2.2	2.2	5.8	10.3	2.7	-0.2	0.1	1.7	0.2
	MU10	31.2	18.5	1.4	1.5	5.9	12.9	15.6	-0.6	-1.3	11.1	21.7
	MU11	50.6	27.5	3.2	3.3	24.4	2.8	7.6	-0.2	0.3	0.4	3.2
	MU12	15.4	12.4	2.6	2.7	3.8	18.0	5.0	-0.1	-0.3	6.3	8.6
	MU13	33.6	20.5	3.4	3.6	1.6	27.0	0.8	0.3	0.0	1.7	1.5
	MU14	2.5	8.8	1.1	1.1	8.2	9.5	3.1	-0.1	-0.3	3.9	7.8
	MU15	2.9	10.8	1.6	1.6	7.0	12.6	1.9	0.1	0.1	1.6	0.6
	MU16	3.5	2.3	1.6	1.6	6.5	7.1	0.8	0.2	0.2	1.3	0.8

3.3. Fat Tissue

The inverse proportionality of BUF and Z_{eq} has been shown in Figure 8, for fat tissue. Moreover, from Table 3 and Figure 9, we observe that all studied parameters, including BUF and PDD distributions, usually reveal close similarities between FA3 and fat tissue. Hence, FA3 can be considered an acceptable TMM for fat tissue in medical physics.

3.4. Lung Tissue

Figure 10 confirms the relationship between the equivalent atomic number and the buildup factor for lung tissue. Furthermore, Table 3 and Figure 11 show that all studied parameters, including BUF and PDD distributions, generally reveal close similarities between LU3 and lung tissue. Therefore, LU3 can be an acceptable TMM for lung tissue for the actual studied photon energy range.

3.5. Muscle Tissue

The observed data in Figure 12 underline the hypothesis of inverse proportionality between BUF and Z_{eq} for muscle tissue. Moreover, Table 3 and Figure 13 show that all studied parameters, including BUF and PDD distributions, usually reveal close similarities between MU8 and muscle tissue. Thus, MU8 can be served as a nearly ideal TMM for

muscle tissue. Moreover, we can consider MU6, MU9 and MU16 as good TMMs for muscle tissue for the actual photon energy range.

Quality assurance and optimization are urgently needed today for textured phantoms used in medical imaging, dosimetry and radiotherapy. Among the existing methods, the usage of 3D-printed customized boluses [25–27] has been introduced as the most promising procedure for TMM fabrication. However, we can consider this study, jointly to our previous work, as an added value for the development of in-house phantoms by offering the easiest formulation and manufacturing process to the scientific community. Furthermore, we will investigate the topic of the search of TMM made of 3D printing materials for nuclear medicine purposes for a photon energy range of 0.015–15 MeV during our next work.

In summary and based on using BUF and a CT number at 30, 100 and 120 kVp for a 0.015–0.15 MeV photon energy interval and on BUF and PDD distributions for a 0.15–15 MeV photon energy interval, we conclude that CB3 and MU8 can be considered as nearly perfect TMMs for cortical bone and muscle tissues, respectively. Additionally, AD1, FA3 and LU3 can be acceptable TMMs for adipose, fat and lung tissues, respectively.

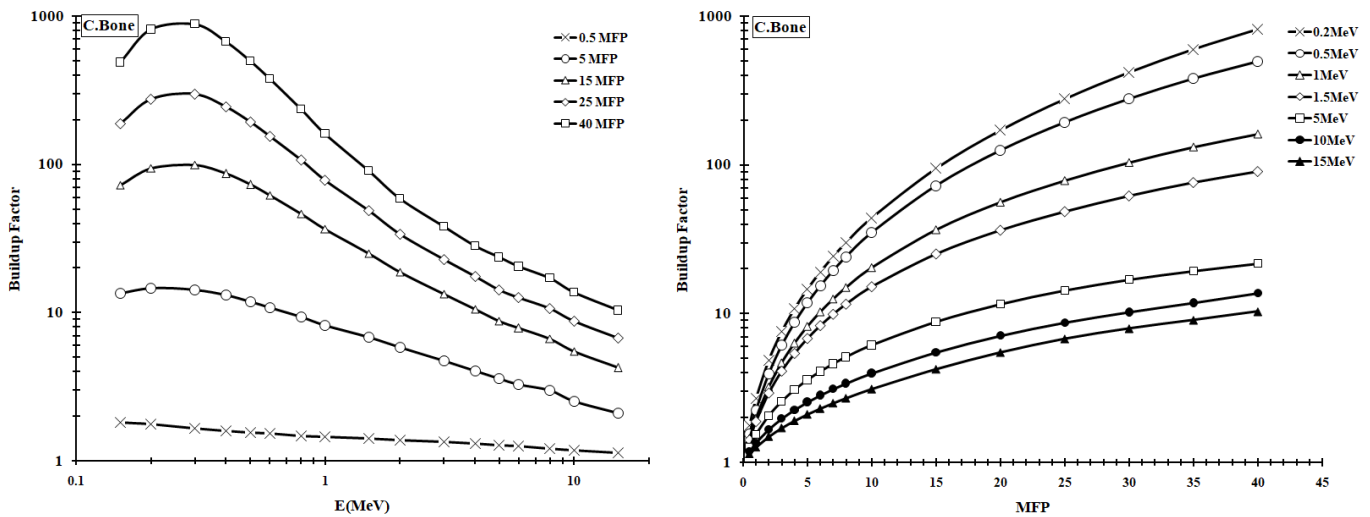


Figure 6. Buildup factor for cortical bone tissue as a function of: (left side) photon energy for fixed depths between 0.5 and 40 mfp and (right side) depth for a fixed photon energy between 0.15 and 15 MeV.

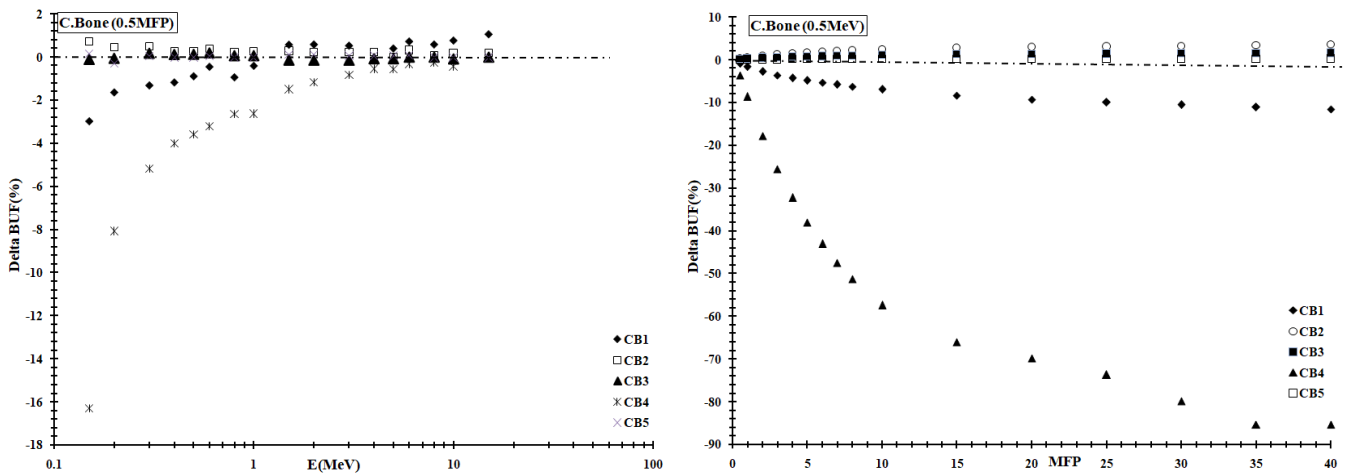


Figure 7. Cont.

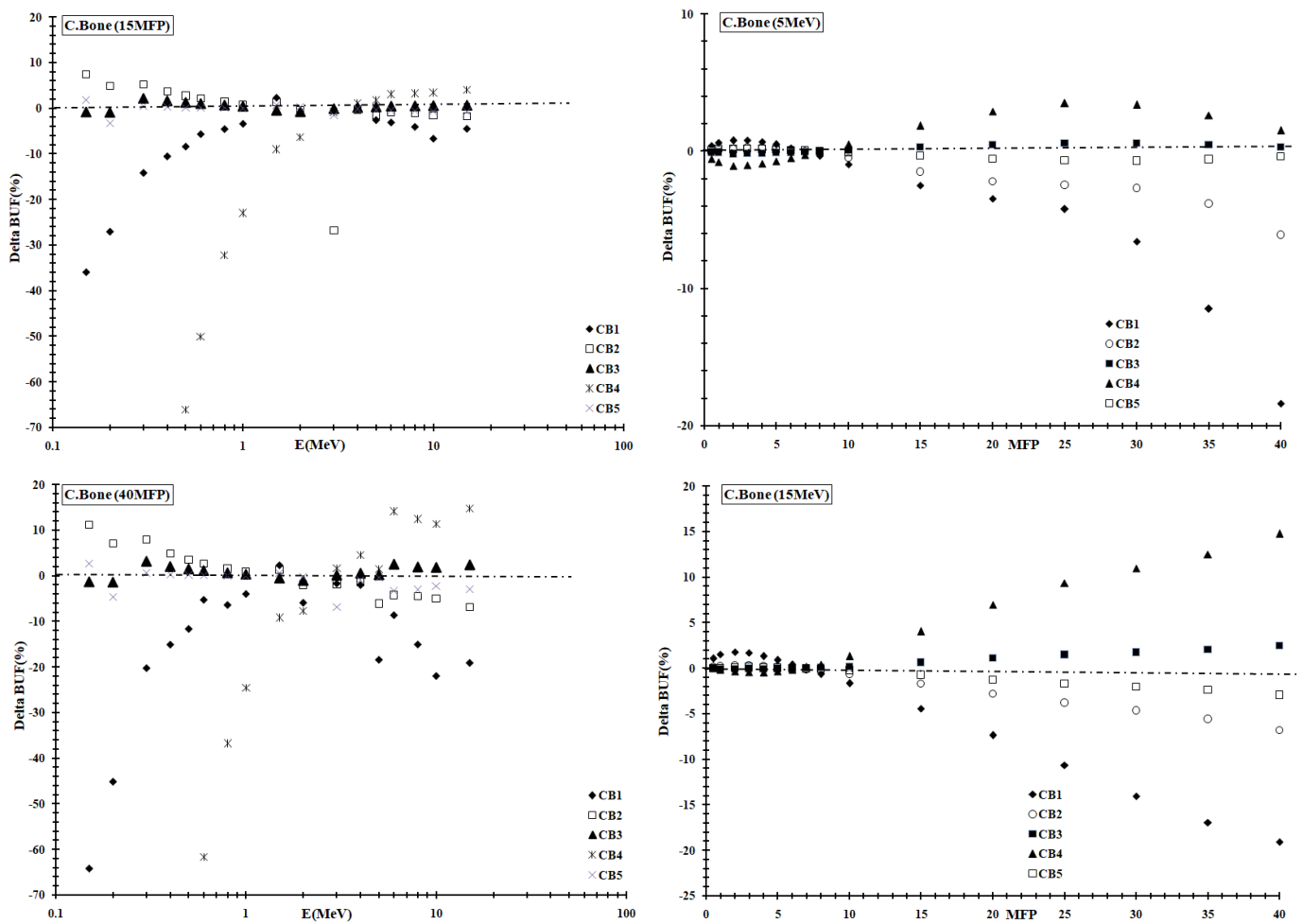


Figure 7. Relative percentage deviation of the BUF value of substitute materials for cortical bone tissue as a function of: (left side) the photon energy for fixed depths of 0.5, 15 and 40 mfp and (right side) depth for fixed photon energies of 0.5, 5 and 15 MeV.

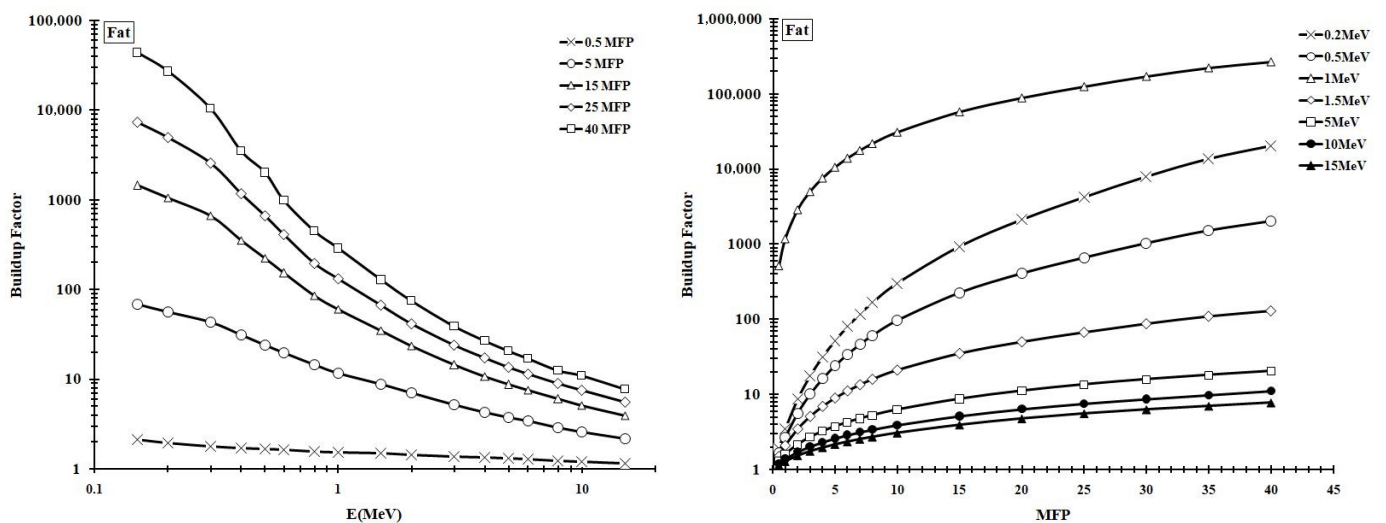


Figure 8. Buildup factor for fat tissue as a function of: (left side) photon energy for fixed depths between 0.5 and 40 mfp and (right side) depth for fixed photon energies between 0.15 and 15 MeV.

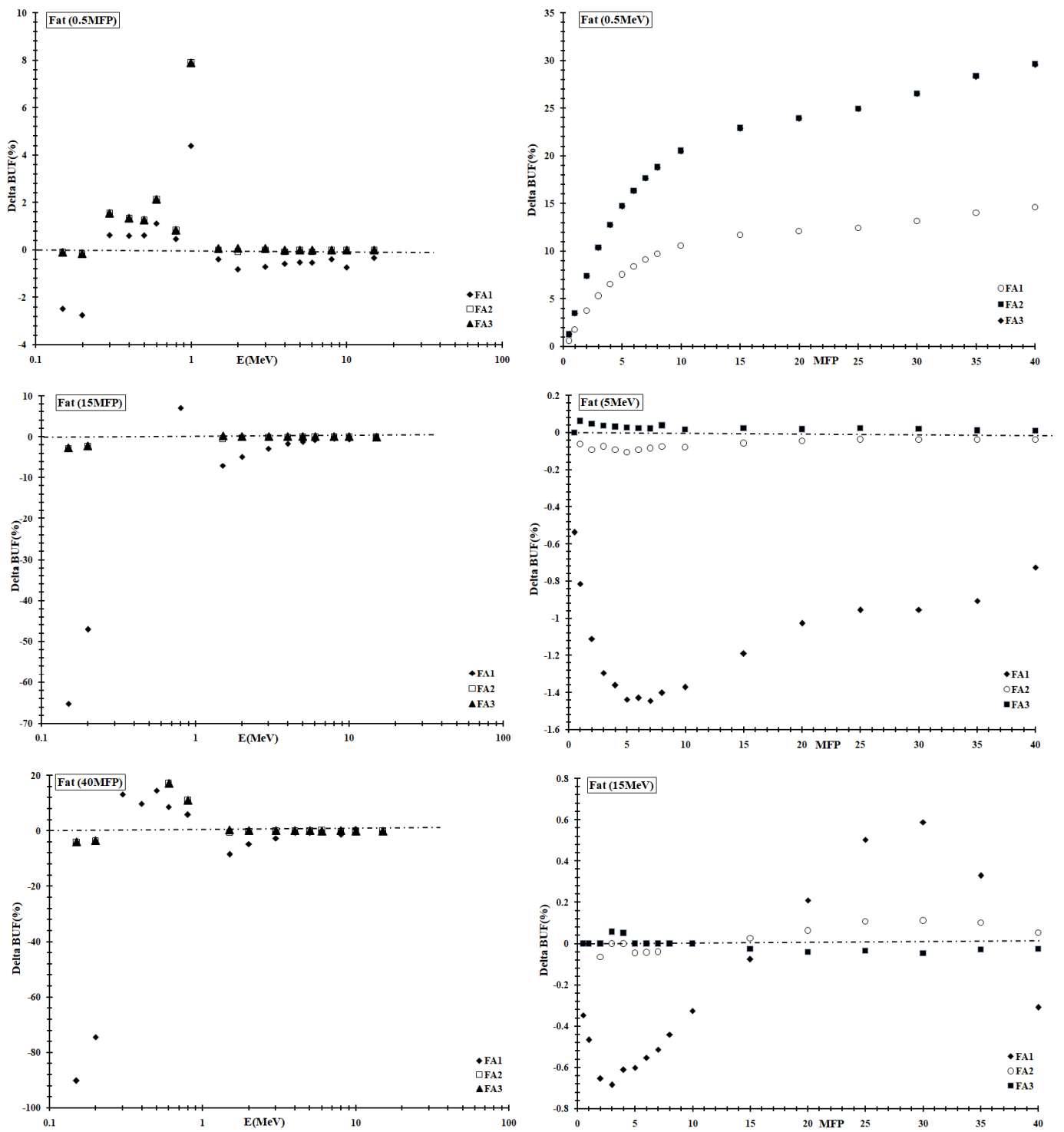


Figure 9. Relative percentage deviation of the BUF values of substitute materials for fat tissue as a function of: (left side) photon energy for fixed depths of 0.5, 15 and 40 mfp and (right side) depth for fixed photon energies of 0.5, 5 and 15 MeV.

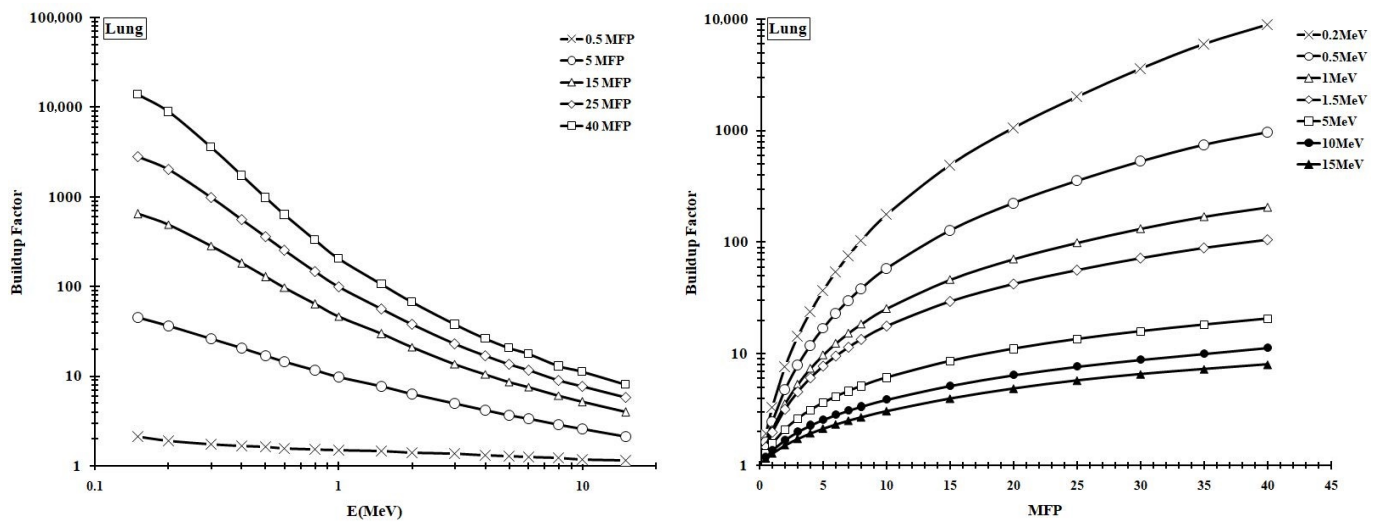


Figure 10. Buildup factor for lung tissue as a function of: (left side) photon energy for fixed depths between 0.5 and 40 mfp and (right side) depth for fixed photon energies between 0.15 and 15 MeV.

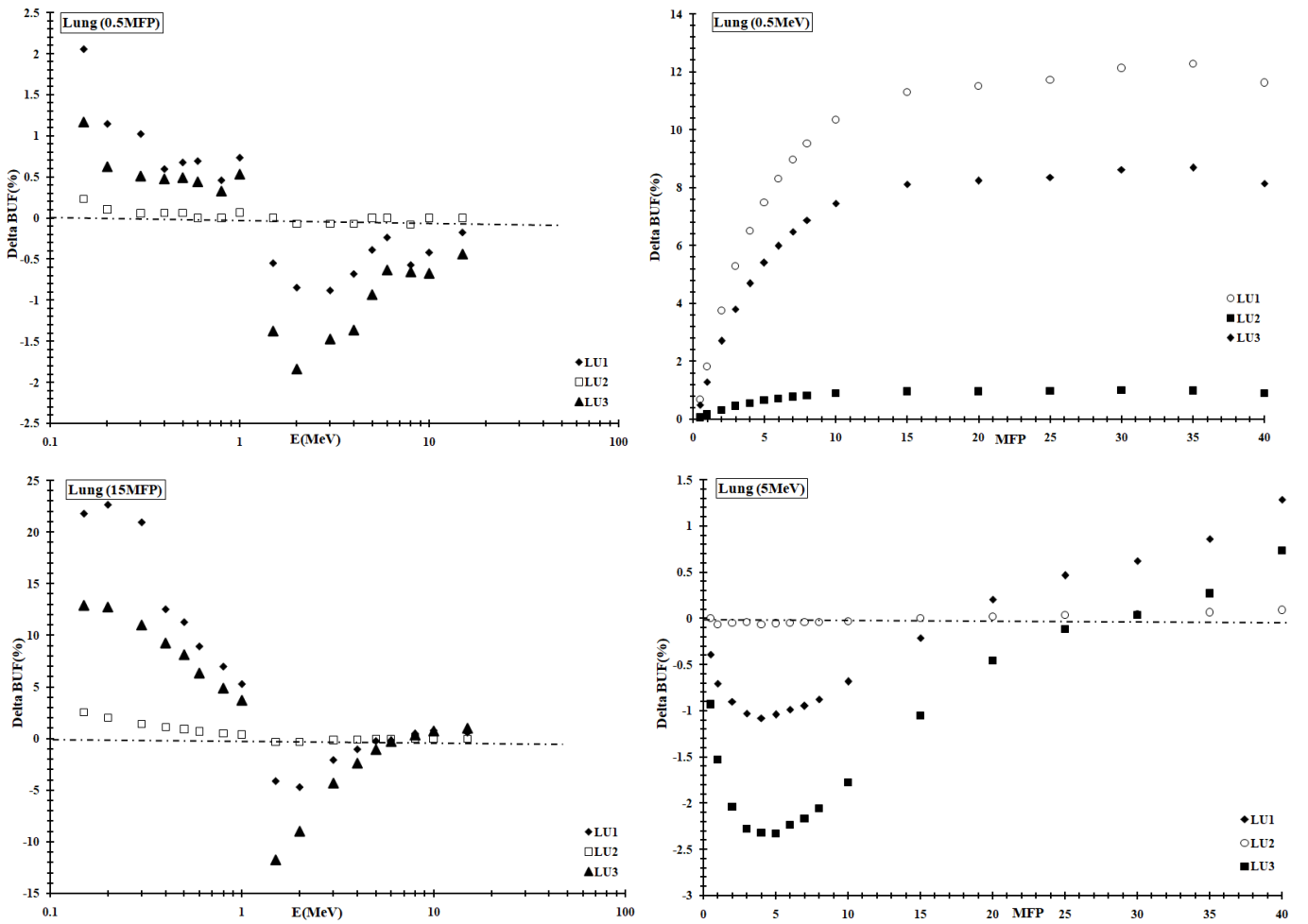


Figure 11. Cont.

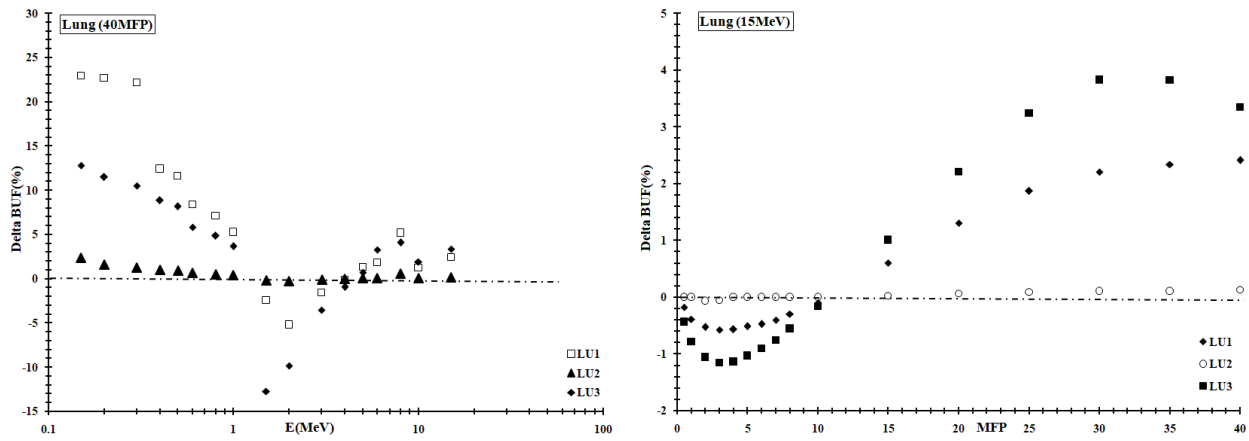


Figure 11. Relative percentage deviation of the BUF values of substitute materials for lung tissue as a function of: (left side) photon energy for fixed depths of 0.5, 15 and 40 mfp and (right side) depth for fixed photon energies of 0.5, 5 and 15 MeV.

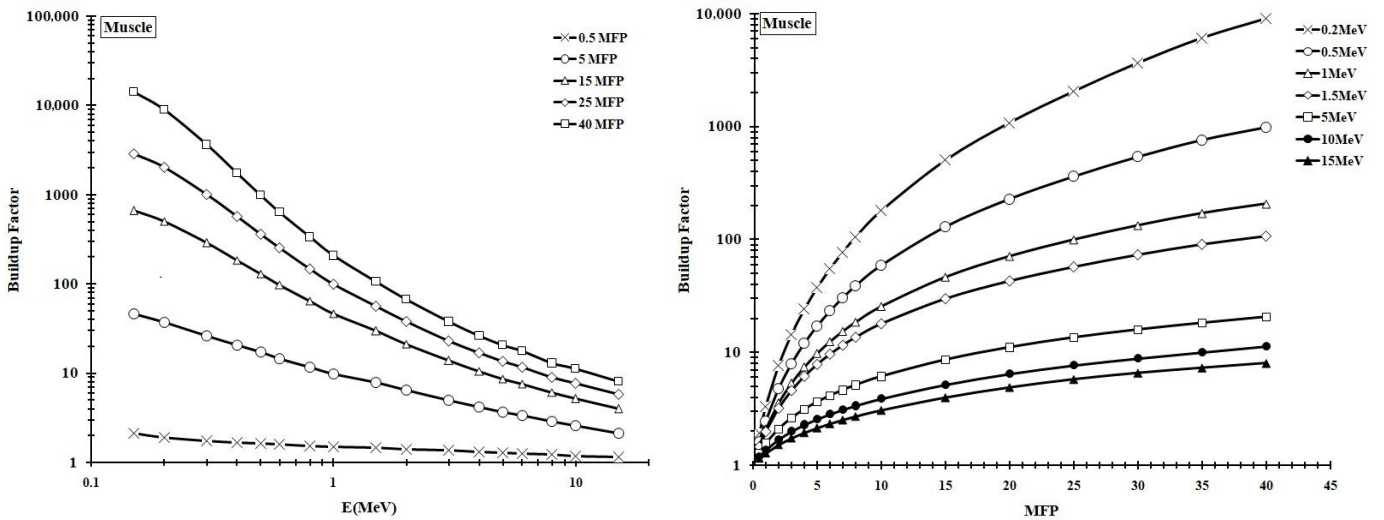


Figure 12. Buildup factor for muscle tissue as a function of: (left side) photon energy for fixed depths between 0.5 and 40 mfp and (right side) depth for fixed photon energies between 0.15 and 15 MeV.

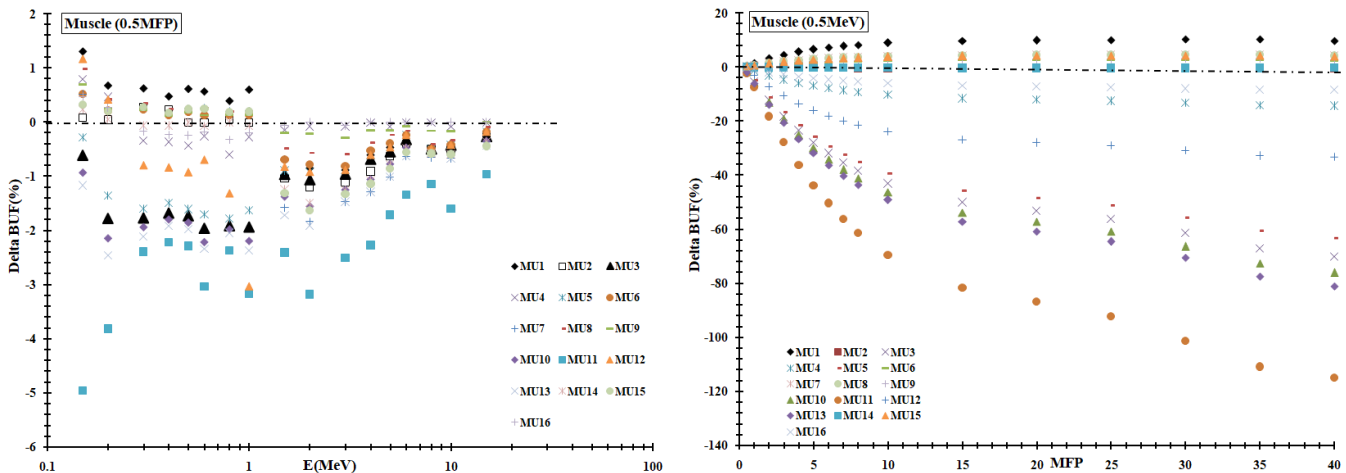


Figure 13. Cont.

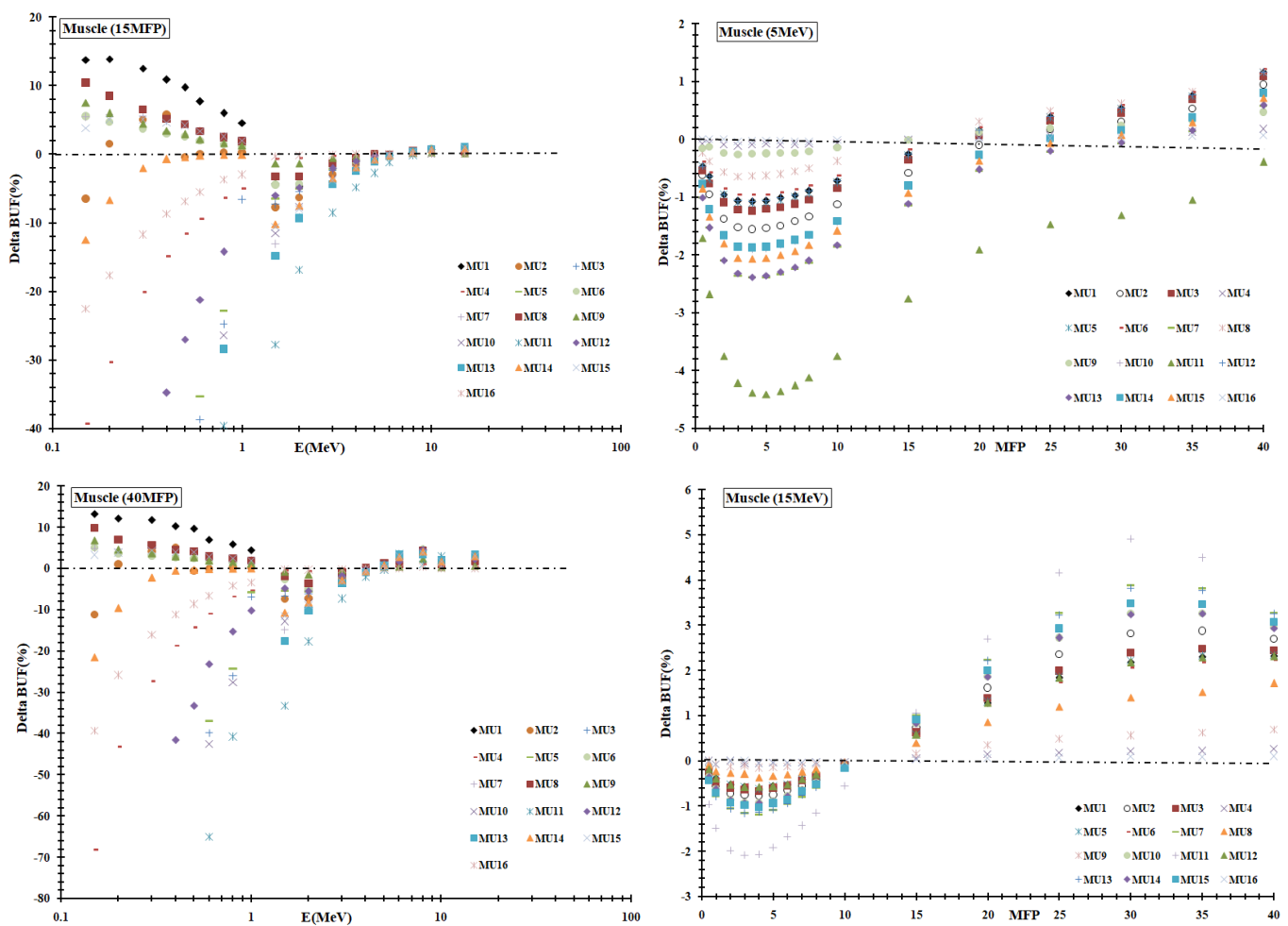


Figure 13. Relative percentage deviation of BUF values of substitute materials for muscle tissue as a function of: (left side) photon energy for fixed depths of 0.5, 15 and 40 mfp and (right side) depth for fixed photon energies of 0.5, 5 and 15 MeV.

4. Conclusions

Currently, medical diagnosis and therapy can be performed using tissue mimicking materials modeling the whole human body or a part of it. In this study, we investigated several radiological properties of human tissues (adipose, cortical bone, fat, lung and muscle) and TMM candidates for a photon energy range of 0.15–15 MeV. In addition to the standard selection criteria of analyzing the attenuation coefficients, we studied the dependence of the buildup factor on photon energy and penetration depths up to 40 mfp. Therefore, we developed an in-house C++ program for BUF computation based on the GP-fitting method. Moreover, we simulated and compared the percentage depth dose distributions of a realistic 6 MV photon beam (with a $10 \times 10 \text{ cm}^2$ field size) through tissues and TMMs using the Geant4 Monte Carlo toolkit. This procedure helped us to distinguish between good and perfect TMM candidates. Consequently, we found that MU8 and CB3 perfectly imitate muscle and cortical bone tissues, respectively. However, AD1, FA3 and LU2 can be suitable for modeling adipose, fat and lung tissues, respectively. Eventually, this study shows that TMMs are beneficial for medical research since they are capable of simulating idealized tissue and allowing the examination of medical devices, procedures and imaging in a test setting without harming animals or humans.

Author Contributions: Conceptualization, methodology, investigation, writing—original draft preparation, writing—review and editing, O.K. and A.A. All authors have read and agreed to the published version of the manuscript.

Funding: This research received no external funding.

Data Availability Statement: Not applicable.

Acknowledgments: The authors extend their appreciation to the College of Applied Medical Sciences Research Center and the Deanship of Scientific Research at King Saud University, Saudi Arabia.

Conflicts of Interest: The authors declare no conflict of interest.

Abbreviations

The following abbreviations are used in this manuscript:

GP	Geometric progression
BUF	Buildup factor
AD1	AP6
AD2	Ethoxyethanol
AD3	Polyethylene
CB1	Aluminum
CB2	P.V.C.
CB3	SB3
CB4	Teflon
CB5	Witt liquid
FA1	Alderson fat
FA2	FT1
FA3	Glycerol trioleate
LU1	Alderson lung
LU2	LN1
LU3	Stacey latex
MU1	Alderson muscle 1
MU2	Alderson muscle 2
MU3	Bakelite
MU4	Goodman liquid
MU5	Lexan
MU6	M3
MU7	Mix D
MU8	MS15
MU9	MS20
MU10	Nylon-6
MU11	Paraffin wax
MU12	Perspex
MU13	Polystyrene
MU14	Shonka plastic
MU15	Temex
MU16	Water

References

- White, D.R.; Constantinou, C. Anthropomorphic phantom materials. *Prog. Med. Radiat. Phys.* **1982**, *1*, 133–193.
- Vasiliev, V.N.; Kostjuchenko, V.I.; Riazantsev, O.B.; Khaybullin, V.G.; Samarin, S.I.; Uglov, A.S. Tissue equivalence of some phantom materials for proton beams. *arXiv* **2010**, arXiv:1005.4389.
- Bradley, D.; Tajuddin, A.A.; Sudin, C.W.A.C.W.; Bauk, S. Photon attenuation studies on tropical hardwoods. *Appl. Radiat. Isot.* **1991**, *42*, 771–773. [[CrossRef](#)]
- Ferreira, C.; Ximenes Filho, R.E.M.; Vieira, J.W.; Tomal, A.; Poletti, M.E.; Garcia, C.A.B.; Maia, A.F. Evaluation of tissue-equivalent materials to be used as human brain tissue substitute in dosimetry for diagnostic radiology. *Nucl. Instrum. Methods Phys. Res. B* **2010**, *268*, 2515–2521. [[CrossRef](#)]
- Marwan, A.; Kabir, N.A.; Hashim, R.; Marashdeh, M.W.; Tajuddin, A.A. Measurement of attenuation coefficients and CT numbers of epoxy resin and epoxy-based Rhizophora spp particle boards in computed tomography energy range. *Radiat. Phys. Chem.* **2018**, *149*, 41–48.
- Yemby, H.T.; Mullisaca P, A.; Apaza V, G.; Chen, F.; Vega R, J. Construction and characterization of materials equivalent to the tissues and organs of the human body for radiotherapy. *Radiat. Phys. Chem.* **2019**, *159*, 70–75.

7. IEC 60601-2-37:2007; Particular Requirements for the Basic Safety and Essential Performance of Ultrasonic Medical Diagnostic and Monitoring Equipment. IEC: Geneva, Switzerland, 2007.
8. Li, P.; Yang, Z.; Jiang, S. Tissue mimicking materials in image-guided needle-based interventions: a review *Mater. Sci. Eng. C* **2018**, *93*, 1116–1131. [[CrossRef](#)]
9. McGarry, C.K.; Grattan, L.J.; Ivory, A.M.; Leek, F.; Liney, G.P.; Liu, Y.; Miloro, P.; Rai, R.; Robinson, A.P.; Shih, A.J.; et al. Tissue mimicking materials for imaging and therapy phantoms: A review. *Phys. Med. Biol.* **2020**, *65*, 1–43. [[CrossRef](#)]
10. White, D.R.; Booz, J.; Griffith, R.V.; Spokas, J.J.; Wilson, I.J. ICRU Report 44: Tissue Substitutes in Radiation Dosimetry and Measurement. *J. ICRU* **1989**, *os23*. Available online: <https://journals.sagepub.com/toc/crub/os-23/1> (accessed on 3 March 2022).
11. Manohara, S.R.; Hanagodimath, S.M.; Gerward, L. The effective atomic numbers of some biomolecules calculated by two methods: A comparative study. *Med. Phys.* **2009**, *36*, 137–141. [[CrossRef](#)]
12. Manohara, S.R.; Hanagodimath, S.M.; Gerward, L.; Subhranshu, S.S. Energy-absorption buildup factors of some fluorides and sulfates: thermoluminescent dosimetric materials. *Mater. Today Proc.* **2019**, *10*, 20–24. [[CrossRef](#)]
13. Kadri, O.; Alfuraih, A. Search for Tissue Equivalent Materials Based on Exposure and Energy Absorption Buildup Factor Computations. *Appl. Sci.* **2022**, *12*, 798. [[CrossRef](#)]
14. Swinehart D.F. The Beer-Lambert Law. *J. Chem. Educ.* **1962**, *39*, 333. [[CrossRef](#)]
15. ANSI/ANS-6.4.3; American Nuclear Society. Standards Committee, Gamma-Ray Attenuation Coefficients and Buildup Factors for Engineering Materials. American Nuclear Society: La Grange Park, IL, USA, 1991. Available online: <https://books.google.com.sa/books?id=jKwYyAEACAAJ> (accessed on 3 March 2022).
16. White D.R. Tissue substitutes in experimental radiation physics. *Med. Phys.* **1978**, *5*, 467. [[CrossRef](#)]
17. Capote, R.; Jeraj, R.; Ma, C.M.; Rogers, D.W.O.; Sanchez-Doblado, F.; Sempau, J.; Seuntjens, J.; Siebers, J.V. Phase-Space Database for External Beam Radiotherapy. Summary Report of a Consultants' Meeting (INDC(NDS)-0484). International Atomic Energy Agency (IAEA). Available online: <http://www-nds.iaea.org/reports-new/indc-reports/indc-nds/indc-nds-0484.pdf> (accessed on 3 March 2022).
18. Cortes-Giraldo, M.A.; Quesada, J.M.; Gallardo, M.I.; Capote, R. An implementation to read and write IAEA phase-space files in GEANT4-based simulations. *Int. J. Radiat. Biol.* **2012**, *88*, 200–208. [[CrossRef](#)]
19. Berger, M.J.; Hubbell, J.H.; Seltzer, S.M.; Chang, J.; Coursey, J.S.; Sukumar, R.; Zucker, D.S.; Olsen, K. *XCOM: Photon Cross Sections Database*; NBSIR 87-3597; National Institute of Standards and Technology: Gaithersburg, MD, USA, 2010. Available online: <https://www.nist.gov/pml/xcom-photon-cross-sections-database> (accessed on 3 March 2022).
20. Kadri, O.; Alfuraih, A. Photon energy absorption and exposure buildup factors for deep penetration in human tissues. *Nucl. Sci. Tech.* **2019**, *30*, 176. [[CrossRef](#)]
21. Jackson, D.F.; Hawkes, D.J. X-ray attenuation coefficients of elements and mixtures. *Phys. Rep.* **1981**, *70*, 169–233. [[CrossRef](#)]
22. Salamaab, E.; Alic, A.S.; Emadd, N.; Radia, A. Validation of GEANT4 Monte Carlo Simulation Code for 6 MV Varian Linac Photon Beam. *Arab. J. Nucl. Sci. Appl.* **2015**, *48*, 70–76.
23. Sardari D.; Maleki, R.; Samavat, H.; Esmaeeli, A. Measurement of depth-dose of linear accelerator and simulation by use of Geant4 computer code. *Rep. Pract. Oncol. Radiother.* **2010**, *15*, 64–68. [[CrossRef](#)]
24. Mia, M.A.; Rahman, M.S.; Purohit, S.; Kabir, S.M.E.; Meaze, A.K.M.M.H. Analysis of Percentage Depth Dose for 6 and 15 MV Photon Energies of Medical Linear Accelerator With CC13 Ionization Chamber. *Nucl. Sci. Appl.* **2019**, *28*, 31–35.
25. Albantow, C.; Hargrave, C.; Brown, A.; Halsall, C. Comparison of 3D printed nose bolus to traditional wax bolus for cost-effectiveness, volumetric accuracy and dosimetric effect. *J. Med. Radiat. Sci.* **2020**, *67*, 54–63. [[CrossRef](#)] [[PubMed](#)]
26. Dai, G.; Xu, X.; Wu, X.; Lei, X.; Wei, X.; Li, Z.; Xiao, Q.; Zhong, R.; Bai, S. Application of 3D-print silica bolus for nasal NK/T-cell lymphoma radiation therapy. *J. Radiat. Res.* **2020**, *61*, 920–928. [[CrossRef](#)] [[PubMed](#)]
27. Lu, Y.; Song, J.; Yao, X.; An, M.; Shi, Q.; Huang, X. 3D Printing Polymer-based Bolus Used for Radiotherapy. *Int. J. Bioprint.* **2021**, *7*, 414. [[CrossRef](#)] [[PubMed](#)]